3-D Indoor Positioning Based on Passive Radio Frequency Signal Strength Distribution

Liangqi Yuan, *Student Member, IEEE*, Houlin Chen, Robert Ewing, *Fellow, IEEE*,
Erik P. Blasch, *Fellow, IEEE*, and Jia Li, *Senior Member, IEEE*

Abstract—In recent years, indoor positioning systems (IPSs) have received attention from many research fields, such as robotics, navigation, human–computer interaction, etc. However, IPS based on passive radio frequency (PRF) technology is still rare. This article proposes a 3-D IPS based on received signal strength (RSS) distribution and Gaussian process regression (GPR). Traditional RSS-based positioning systems have a transmitter with known frequencies, while in the proposed PRf signal of Opportunity—3D IPS (PRO-3DIPS), the system neither deploys new transmitters nor uses any a priori knowledge of transmitters. Furthermore, PRO-3DIPS integrates multiple Signal of Opportunity (SoOP) sources, shadowing, fading, and also captures scenario signatures. Data collection and analysis of PRF-based RSS distribution in 3-D space enables the capability of 3-D positioning. Three methods are applied and compared to find the frequency band most impacted by the scenario to achieve the best positioning performance as well as used in the estimation of RSS distribution. The RSS distribution is estimated by measuring the PRF spectrum on a fixed grid in the scenario. Using the RSS distribution, the GPR can accurately locate the receiver position. RSS at 90-gridded positions were collected in the experiment scenario, with one hundred samples at each position. The experimental result shows that a root-mean-square error (RMSE) of the proposed PRO-3DIPS is 0.292 m when the sampling distance is 1 m. The result demonstrates that the PRF spectrum is a new modality for the positioning task, which demonstrates better performance than most existing RF-based technologies.

Index Terms—Gaussian process regression (GPR), indoor positioning system (IPS), passive radio frequency (PRF), received signal strength (RSS) distribution, Signal of Opportunity (SoOP).

I. INTRODUCTION

WITH the development of smart life and industrial automation, an accurate, low latency, and low-cost

Liangqi Yuan was with the Department of Electrical and Computer Engineering, Oakland University, Rochester, MI 48309 USA. He is now with the School of Electrical and Computer Engineering, Purdue University, West Lafayette, IN 47907 USA (e-mail: liangqiyuan@oakland.edu).

Jia Li is with the Department of Electrical and Computer Engineering, Oakland University, Rochester, MI 48309 USA (e-mail: li4@oakland.edu).

Houlin Chen is with the Faculty of Arts and Science, University of Toronto, Toronto, ON M5S 1A1, Canada (e-mail: houlin.chen@mail.utoronto.ca).

Robert Ewing is with the Sensors Directorate, Air Force Research Laboratory, Wright-Patterson AFB, OH 45433 USA (e-mail: robert.ewing.2@us.af.mil).

Erik P. Blasch is with the Information Directorate, Air Force Research Laboratory, Rome, NY 13441 USA (e-mail: erik.blasch.1@us.af.mil).

Digital Object Identifier 10.1109/JIOT.2023.3263476

indoor positioning system (IPS) has always been desirable to enable position-based services. Due to the relatively complex indoor scenarios, including multiple interference sources, building structures, and weak GPS signals, some indoor positioning solutions have been proposed, such as WiFi [1], [2], visible light [3], [4], ultra wide band (UWB) [5], [6], radio frequency identification (RFID) [7], [8], broadcasting [9], magnetic field [10], etc. IPS based on active radio frequency (RF) signals, such as WiFi, UWB, and RFID are the most popular research directions of IPS, benefiting from its advantages of low-power consumption, high precision, and low cost. However, the positioning system using passive RF (PRF) technology based on multiple Signals of Opportunity (SoOPs) is still a blank field.

A. Motivation and Proposed Solution

RF-based IPSs usually consist of a transmitter, target, and receiver. These RF signal information can also be divided into received signal strength (RSS) indicator and channel state information (CSI) according to whether they contain phase information represented by the angle. The RSS-based positioning system has attracted our attention because of its lower cost, strict requirements, and robustness of the instrument. However, RSS-based positioning systems also face many problems, including shadowing, multipath, diffraction, etc. [11], [12]. A common solution for IPS based on RF signal RSS is triangulation, which needs additional transmitters to determine the target position and real-time synchronization. However, the triangulation solution still has limitations in the number of devices and performance.

Fading of the wireless channel has a significant impact on the proposed system performance, including large-scale fading and small-scale fading, where these two fadings are spatially, temporally, and frequency related [13]. The fadings from multiple RF signal sources are used to feature the PRF spectrum, including large-scale fading due to long distances and large objects, such as buildings and spatially small-scale fading due to the constructive and destructive effects at the wavelength-level. Temporally small-scale fading exhibits a Rayleigh distribution, which can be approximated by a Gaussian distribution when the sample size is large [14], so Gaussian processes are used to model small-scale fading. Frequency selective small-scale fading is also a crucial factor, so it is necessary to consider fading to find the most impacted frequency band to achieve the positioning task. Due

Fig. 1. Block diagram of the proposed PRF sensor-based positioning system PRO-3DIPS.

TABLE I
COMPARISON OF PRF AND WiFi POSITIONING SYSTEM

Positioning System	PRF	WiFi
Mechanism	RSS (SoOP fading fingerprinting)	RSS (Multilateration; finger-printing); CSI (AoA; ToF)
Frequency Range	Full frequency band	2.4 GHz; 5 GHz
Device	One receiver only	Several APs and receiver
Price	$\sim$ \$30 (RTL2832U)	Depends on APs
Performance	Depends on scenario, task, and frequency	Depends on APs number and locations
3D Positioning Capability	Naturally available	Additional APs required
Large-scale Application	More frequency required	More APs required
Customizability	Customizable frequency	Customizable APs number and locations
Power Consumption	Low	High (signal transmission)
Application Restrictions	Not valid in signal shielding scenarios	Negligible

AP refer to access point; AoA refer to Angle of Arrival; ToF refer to Time-of-Flight.

TABLE II
INDOOR POSITIONING TECHNIQUES AND PERFORMANCE OF RF

Reference	Technology	Regression Algorithm	Area (m^2)	Sample Distance (m)	RMSE (m)
[21]	WiFi	GPR	15.6×16.3	0.5	1.29
[28]		GPR	23.2×25.6	1.6	5.12
[29]		GPR	13×29	2	0.96
[30]		SVR	21.3×31.8	2	1.48
[31]		k-NN	16×21	2	0.66
[32]		k-NN	18×50	1	0.80
[33]		DL	16×32	1.5	1.79
[34]		DL	35×50	20	3.68
[8]	RFID	SVR	5.6×5.6	0.6	0.20
[23]		k-NN	3.6×4.8	0.4	0.15
[35]	Bluetooth	Polynomial Regression	40×60	18	2.44
			40×60	9	1.74
[36]	USRP	Neural Network	3×5	0.2	0.10
				0.4	0.32
				0.6	0.39

to the assumed long distance between the SoOP source and the experiment location and the slow movement of the receiver in the indoor scenario, the near-far effect, and the Doppler effect can be ignored.

This article proposes that the IPS implemented with the PRF technology is an important supplement, extension, and inspiration. The PRF signal and the SoOP are inseparable. The PRF signal not only includes SoOP but also an extension to SoOP. SoOP aim to utilize nontarget or nontask signals to achieve tasks [15], [16], [17], such as navigation tasks using cellular network, WiFi, broadcasting, communication satellite, etc. The PRF spectrum is not only a utilization of the SoOP but it also capture the scenario signature, such as building structures, metallic objects, liquids, humans, and nontarget RF signals. In addition, the PRF spectrum can also capture multisource multipath, large-scale fading, and small-scale fading as features. Therefore, we propose a utilized PRF SoOP and captured scenario information 3-D IPS (PRO-3DIPS). Fig. 1 shows an imaginary PRO-3DIPS capturing multiple SoOP sources and scenario signatures, which is able to find the most impacted frequency bands and then achieve high-precision positioning. Compared to active RF technologies, such as WiFi that utilize SoOP, PRF sensing only requires a receiver and does not rely on any specific equipment or local transmitter to achieve indoor positioning. It is worth noting that the PRF technology does not apply any SoOP prior, and it is not limited to any frequency band of SoOP, which enables PRF to use any SoOP that are beneficial to the task. Therefore, the PRF spectrum is capable of capturing biological information, building structures, targets, etc., in the scenario, and can feature multiple RF signal sources, multipath, and multifading. Table I shows the comparison of the characteristics of PRF and active RF positioning system with WiFi as an example.

B. Related Work

We summarize the relevant RF-based IPS in terms of technology, experimental setup, and performance. Positioning problems in machine learning are usually regression methods rather than classification or clustering tasks because they require specific coordinates. For the regression problem of positioning, machine learning is a common solution in recent literature [18], such as support vector regression (SVR) [19], [20], Gaussian process regression (GPR) [21], [22],

k-Nearest Neighbor (k-NN) [23], [24], as well as deep learning (DL) [25], [26], etc. Table II summarizes some works utilizing RF technologies and regression algorithms, as well as their performance. The performance of IPS is usually evaluated by the root-mean-square-error (RMSE) of the observation coordinates and the predicted coordinates. Probability density function (PDF) and cumulative distribution function (CDF) of positioning are also a common evaluation metrics because they intuitively present the changing trend of errors and confidence levels [27].

3-D IPS is a more challenging task, and a general solution does not yet exist. A popular method is computer vision (CV) or light detection and ranging (LiDAR)-based simultaneous localization and mapping (SLAM) [37], [38]. Although SLAM is a proven method, it suffers from its high cost and high requirement for computing resources. 3-D IPS based on RF technologies, such as WiFi and RFID is still in its infancy. Chen et al. [39] proposed a WiFi-based semi-supervised

machine learning method that achieves positioning by comparing the distance between the user and transmitters, which are placed at different heights. Another WiFi-based method [40] proposes 3-D positioning through azimuth and elevation AoA estimation in CSI. However, this method also requires the cooperation of multiple transmitters and the error increases as the number of transmitters decreases. Moreover, [41] proposes a fake RFID-based 3-D IPS that adds additional antennas in the vertical direction. Although it has a surprising error that RFID IPSs usually have, it is evident that it cannot be extended to a general case since it cannot add antennas in the vertical direction without limit. Our proposed PRF system does not have a series of drawbacks that exist in the related literature and also achieves fairly comparable performance. Even more commendable is that the PRF system is an innovative modality used in 3-D positioning tasks.

C. Previous Work and Contributions

In our previous work, PRF sensing technology has achieved some remarkable results on human sensing, such as human occupancy detection [42], authentication [43], [44], activity recognition [45], and positioning [46]. These works achieve human sensing using the RF spectrum of human signatures, which is based on the sensitive nature of RF signals to liquids. Previous work [46] introduced a PRF-based human positioning method, which fixes six PRF sensor antennas and collects human spectrum data at different positions in the scenario to achieve human positioning. However, this article changes the target of interest from a human to the RSS distribution of the scenario. We use the RF spectrum of the scenario signature to implement IPS that other researchers regard as noise.

Since the PRF sensing technology does not use any a priori knowledge of any transmitters, the PRF sensor is not limited to any specific receive frequency. Although it is feasible to use the collected full-band PRF spectrum for positioning, too many features consume resources, decrease accuracy, and decrease sampling rate, which is not ideal for a real-time IPS. Therefore, finding the frequency in the specific scenario with the most impact is one of the most critical factors affecting regression accuracy. For data dimensionality reduction methods, common solutions include principal component analysis (PCA), factor analysis (FA), independent component analysis (ICA), etc. [47], [48]. Previous work [42] used the PCA algorithm to find several human-sensitive frequency bands from the full frequency band. Compared to PCA, which shows the features with the most significant variance, explainable artificial intelligence (xAI) technologies provide another solution for the relationship between the input and output of a machine learning model. SHapley Additive exPlanations (SHAPs) [49] provides interpretability, visualization, and interactivity of the model output, which gives us another choice for finding the most impact frequency band.

The work reported in this article demonstrates a high precision PRO-3DIPS. SHAP is used to find the most impact PRF band. After targeted sampling of this particular frequency band, a 3-D RSS distribution is demonstrated. After the parameterization, analysis, and modeling of GPR to the 3-D RSS distribution, our positioning framework is validated as an accurate, reliable, and low-power consumption solution. The contributions of this article are:

1) Observation, comparison, and character study are implemented for the PRF spectrum in different positions. SHAP, PCA, and statistic variance are used to find the frequency band most impacted by the scenario that differentiates the PRF spectrum at various positions.
2) RSS distribution of a 90-gridded position spectrum is collected in an indoor scenario at the most impacted frequency band. To the best of our knowledge, this is the first paper to sample, observe, and compare indoor RSS distribution in 3-D space and at different frequencies.
3) GPR conforming to 3-D positioning and PRF spectrum is established, parameterized, and trained. The proposed GPR with Matern kernel regressor can lead to positioning performance of 0.292 m in RMSE, 0.987 in coefficient of determination R^2, and 0.546 m in 95% confidence error (CE). The achieved performance highlights PRF technology as a new modality for indoor positioning, and it is worth commenting that it is inherently endowed with the capability of 3-D positioning.

The presentation of this work is as follows. Based on observations of the current state of RF sensing technology and solutions to regression problems, the methodology of PRO-3DIPS is described in Section II. Section III presents the experimental setup, phenomena, and results. Some discussions of the experimental results and comparisons with the state-of-the-art are given in Section IV prior to the conclusions and future research in Section V.

II. METHODOLOGIES

This section introduces the proposed 3-D IPS, including a software-defined radio (SDR)-based PRF technology, frequency band selection algorithm, GPR, and three evaluation criteria.

A. Passive Radio Frequency Technology

PRF technology is one of the core technologies in PRO-3DIPS. PRF system passively receives ambient RF signals in the scenario. It neither deploys new transmitters nor transmits, rejects, shields, and is unaware of RF signals. PRF system also does not use any a priori information about the possible existence of RF transmitters. PRF technology has many advantages, including low cost, harmless, customized frequency band selection, etc. SDR is a common technique to control the parameters of PRF sensor at the software level, such as frequency range, step size, sampling rate, number of samples in in-phase and quadrature (IQ) data, etc. Therefore, the low-cost RTL-SDR RTL2832U was chosen as the PRF sensor to passively receive the spectrum, as shown in Fig. 2.

The center frequency range $\mathbb{B}$ is set from 24 to 1000 MHz, with a sampling step size of 2.4 MHz, a bandwidth of 1.2 MHz, and a sampling rate of 2.4 MHz. At the center frequency f determined by each sampling step, the sample number N of 4096 IQ data were collected, respectively. The

Fig. 2. RTL-SDR RTL2832U DVB-T tuner dongle and antenna used to passively receive the spectrum.

sampling time for each center band is about 2 ms. The average power P in dB at each center frequency, which is also the PRF spectrum used in our experiments, can be calculated as

$$P(f) = 10 \log_{10} \frac{\sum_{i=1}^{N} p_f(i)}{N/2} \tag{1}$$

where the average spectrum power P is a function of the center frequency f. p_f is the power at each center frequency f and can be calculated from IQ data

$$p_f = \frac{V_f^2}{R} \tag{2}$$

where V_f is the voltage data at the center frequency f. R is a typical input impedance, rated at 50 Ω by the RTL2832U. IQ data are collected alternately by SDR, and voltage data V_f can be obtained by the raw 8-bit quadrature IQ pair I_f and Q_f

$$V_f = \frac{\sqrt{I_f^2 + Q_f^2}}{255/2} - 1. \tag{3}$$

Therefore, we can establish the following mathematical model, for n pairs of observations will be given by D and C

$$C = Dw + \varepsilon \tag{4}$$

where $w \in \mathbb{R}^{m \times 3}$ is a transform matrix between the observed data set $D \in \mathbb{R}^{n \times m}$ and the observed coordinate set $C \in \mathbb{R}^{n \times 3}$ of the GPR model. $\mathbb{R}$ is the set of real numbers. D and C are from the PRF spectrum $P(f)$ and the corresponding 3-D coordinates, respectively, which are defined as

$$d_i = \{P_i(f_1), P_i(f_2), \ldots, P_i(f_m) | f \in \mathbb{B}, m \in \mathbb{N}\}_i, \tag{5}$$
$$c_i = (x, y, z)_i \tag{6}$$

where d_i is the ith sample of set D, and c_i is the corresponding coordinate. $\mathbb{N}$ is the set of natural numbers. (x, y, z) is the 3-D coordinate corresponding to abscissa, ordinate, and applicate, respectively. The Gaussian additive white noise present in the system is represented by ε, which is independent and identically distributed (i.i.d.) Gaussian distribution with zero mean and variance σ_n^2

$$\varepsilon \sim \mathcal{N}\left(0, \sigma_n^2\right). \tag{7}$$

B. Frequency Band Selection

Frequency band selection is necessary for PRF sensing technology. Dimensionality reduction or feature extraction techniques are not used in the proposed PRO-3DIPS because the physical meaning in the original data needs to be preserved for further analysis. The PRO-3DIPS method selects some frequency bands from the full frequency band for data collection and regression tasks, since they can effectively save data collection time, economize resources, and improve regression accuracy. Depending on different tasks and scenarios, the frequency band selected differs. In previous work [42], the human sensitive frequency band was found to be around 500 to 700 MHz. The frequency band selection algorithm aims to find the frequency band with the most impact, which is a precondition of achieving regression. SHAP, PCA, and statistical variance are used to find the most impact frequencies, respectively.

PCA is one of the essential dimensionality reduction methods, which replaces the original data by finding the most impact features in the data with eigenvector selections. PCA is used in this article only to select some of the most impact frequencies. Common PCA toolkit such as Scikit-learn uses singular value decomposition (SVD) to find the most impact components in feature space. The features corresponding to the most significant variance are additionally used for secondary verification. In addition to PCA and statistical variance, a common solution is to use SHAP to find the most impact frequencies. SHAP is a game-theoretic approach to interpreting the output of a machine learning model. SHAP supports visualization and interpretability of features, so SHAP has also become one of the solutions to find the most impact frequencies.

The selected frequency band is worth investigating in the experiment. According to our observations and previous work [42], the most impacted frequency bands are multiple randomly distributed over the whole frequency band. Each frequency band will include one or several of the most impacted frequencies. In this work, we only want to select a single frequency band containing several consecutive frequencies. A single frequency band can not only limit sampling time and save computational resources but also achieve comparable accuracy, be easy to implement, and provide prior knowledge for further work. Therefore, the selected frequency band $\mathbb{B}_s$ can be obtained by SHAP, PCA, and statistical variance. Specifically, the SHAP, PCA, and statistical variance methods first obtain the most impacted frequency sets $\mathbb{B}_{\text{SHAP}}$, $\mathbb{B}_{\text{PCA}}$, and $\mathbb{B}_{\text{Var}}$, respectively. First, calculate the weight of each frequency in $\mathbb{B}_i$, which is equal to the sum of the impact of the three methods. Second, calculate the weight of each $\mathbb{B}_i$ set, which is equal to the sum of the impact of the frequencies. Finally, compare all the $\mathbb{B}_i$ weights to get the set with the most impact, i.e., $\mathbb{B}_s$. The algorithm of frequency band selection has been summarized in Algorithm 1.

C. Gaussian Process Regression

After selecting the frequency band $\mathbb{B}_s$ in Algorithm 1, we recollected the data in this particular selected frequency

Algorithm 1 Frequency Band Selection

Input: D, C
Output: $\mathbb{B}_s$
 $\mathbb{B}_{\text{SHAP}} \leftarrow \text{SHAP}(D, C)$
 $\mathbb{B}_{\text{PCA}} \leftarrow \text{PCA}(D)$
 $\mathbb{B}_{\text{Var}} \leftarrow \text{Var}(D)$
 for $i \leftarrow 1$ **to** $m - 4$ **do**
  $\mathbb{B}_i \leftarrow \{f_i, f_{i+1}, f_{i+2}, f_{i+3}, f_{i+4}\}$
  $\text{Sim}_i \leftarrow \text{Similarity of } \mathbb{B}_i \text{ and } \{\mathbb{B}_{\text{SHAP}}, \mathbb{B}_{\text{PCA}}, \mathbb{B}_{\text{Var}}\}$
 end for
 $s \leftarrow \underset{i}{\text{argmax}} \, \text{Sim}_i$
 $\mathbb{B}_s \leftarrow \{f_s, f_{s+1}, f_{s+2}, f_{s+3}, f_{s+4}\}$

band to implement GPR. For a concise presentation, all D in this section are data collected on $\mathbb{B}_s$. The 3-D positioning task based on the PRF spectrum can be considered as solving a GPR problem with multiple inputs and multiple outputs. Following the introduction and analysis of GPR in [50] and [51], we build a mathematical model based on the PRF data. According to Bayesian Inference, the posterior distribution is given as

$$p(w|D, C) = \frac{p(C|D, w)p(w)}{p(C|D)}. \tag{8}$$

The derivation of the posterior distribution $p(w|D, C)$ is elaborated and derived in [50]. According to the posterior distribution of w and given D and C, the corresponding approximate coordinates $\hat{C}' \in \mathbb{R}^{n' \times 3}$ can be obtained from $D' \in \mathbb{R}^{n' \times m}$. Under the assumption that the data can be expressed as a joint Gaussian distribution with zero mean and covariance given by

$$\begin{bmatrix} C \\ \hat{C}' \end{bmatrix} \sim \mathcal{N}\left(0, \begin{bmatrix} K & K' \\ K' & K'' \end{bmatrix}\right). \tag{9}$$

where K, K', and K'' are defined as

$$\begin{aligned} K &= D^T \Sigma_w D \\ K' &= D'^T \Sigma_w D = D^T \Sigma_w D' \\ K'' &= D'^T \Sigma_w D'. \end{aligned} \tag{10}$$

According to the assumption of transform matrix $w \sim \mathcal{N}(0, \Sigma_w)$, the mean and covariance of C and $\hat{C}'$ equal to

$$\begin{aligned} \text{E}(D'w) &= D'\text{E}(w) = 0 \\ \text{cov}(Dw, D'w) &= \text{E}[(Dw)(D'w)] = K'. \end{aligned} \tag{11}$$

It can be seen that the covariance $\text{cov}(Dw, D'w)$ gives the GPR model the ability to distinguish between the observation data D and the predictive data D', which can predict corresponding approximate coordinate $\hat{C}'$. The kernel K' is used to provide the similarity between two data vectors. This similarity measure provides the basis for GPR theory, which takes into account several aspects, including correlation with other components, anisotropy, periodicity, etc. The corresponding approximate coordinates $\hat{C}'$ from the predictive data set can be obtained by

$$\hat{C}' = K'\left(K + \sigma_n^2\right)^{-1} C. \tag{12}$$

Some kernels commonly described in GPR [50], [51] are also selected for consideration, including the radial basis function (RBF) kernel k_{RBF}, rational quadratic (RQ) kernel k_{RQ}, exponential sine squared (ESS) kernel k_{ESS}, and Matern kernel k_M. These four kernels have similar functional forms, which can be expressed as

$$k.\left(d, d'|\sigma^2, l\right) \in K' \tag{13}$$

where $k.$ represents different GPR kernels, d is a sample vector of observation data set D, d' is a sample vector of predictive data set D', the two hyperparameters are σ^2 is variance and $l \in \mathbb{R}^{1 \times m}$ is length scale vector. It is necessary that l is set to be anisotropic because all features in d have different properties, which is confirmed by the RSS distribution experiments, as shown in Figs. 6 and 7. Also, the upper and lower bounds of l need to be strictly set according to prior knowledge. Because when l is set too large, the fitted model will ignore some details in the data and lead to underfitting, while if l is set too small, the fitted model will be too detailed and lead to overfitting. Noise in the model is usually explained by the white kernel, which explains noise in the data as i.i.d.

$$k_N\left(d, d'\right) = \begin{cases} \text{noise level}, & \text{if } d = d' \\ 0, & \text{o.w.} \end{cases} \tag{14}$$

where the hyperparameter noise level reflects the noise in the data. The white kernel is usually added with other kernels as the total kernel of the GPR model. Choosing a suitable kernel is crucial for the fitting of the GPR model, which effectively improves the accuracy and robustness of the model. A common GPR kernel solution is the additive form of these single kernels above. GPR can automatically fit these kernels and optimize the parameters, respectively. Although the multiparameter of multikernel provides room for model optimization, the increase in computational complexity may lead to excessive resource consumption for model fitting.

For positioning problems, the evaluation criteria usually have RMSE to determine the Euclidean distance between true and predicted coordinates

$$\text{RMSE} = \sqrt{\frac{\left\|C' - \hat{C}'\right\|_2^2}{n'}}. \tag{15}$$

Coefficient of determination R^2 determines the relationship between data D', its predicted coordinate $\hat{C}'$, and true coordinate C' in the GPR regression relationship, that is, the proportion of $\hat{C}'$ that can be explained by the D'. In simple terms, if the average power collected at the same coordinates is unchanged, then, the degree of variation of the coordinates will decrease by R^2

$$R^2 = 1 - \frac{\left\|C' - \hat{C}'\right\|_2^2}{\left\|C' - \overline{C'}\right\|_2^2} \tag{16}$$

where $\overline{C'}$ is the mean vector of C'. F is the CDF of RMSE, which can intuitively reflect the speed of RMSE accumulation. F is also an essential evaluation criterion for positioning

Algorithm 2 Kernel Selection

Input: D, C, D', C'
Output: kernel
1: **for** ker **in** $\mathcal{P}\big(\{k_{\text{RBF}}, k_{\text{RQ}}, k_{\text{ESS}}, k_M\}\big) + k_N$ **do**
2:     $\hat{C}'_{(\text{ker})} \leftarrow K'_{(\text{ker})}\big(K + \sigma_n^2\big)^{-1} C$ ▷ (12)
3:     $\text{Score}_{(\text{ker})} \leftarrow \text{RMSE}_{(\text{ker})} + (1 - R^2_{(\text{ker})})$
             $+ \text{CE}_{(\text{ker})}$ ▷ (15), (16), (17)
4: **end for**
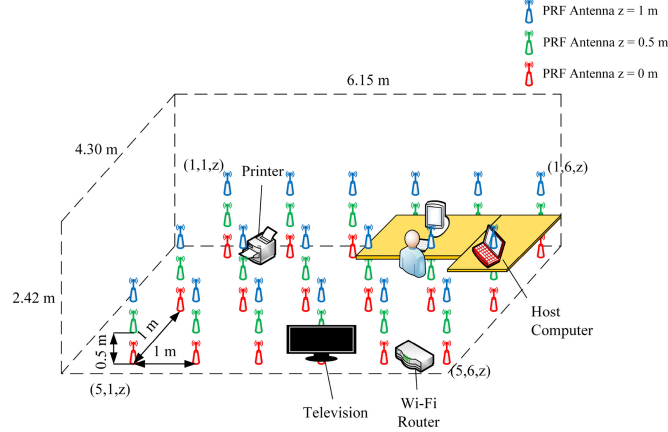5: kernel $\leftarrow \underset{\text{ker}}{\text{argmax}} \ \text{Score}_{(\text{ker})}$

Fig. 3. Illustration of the experiment scenario used to collect the PRF spectrum. The red, green, and blue antennas are represented as 0, 0.5, and 1 m from the bottom of the antenna to the ground, respectively. Only a part of the coordinates of the PRF antenna are marked in the figure.

tasks, especially those with strict requirements. The error corresponding to the confidence will be used as a numerical representation of the error. The CE as

$$\text{CE} = F_{\text{RMSE}}^{-1}(\gamma) \tag{17}$$

where γ is confidence level, the typical confidence level usually can be set as 90%, 95%, 99%, etc. The GPR model establishment and kernel optimization have been detailed in Algorithm 2, where power set $\mathcal{P}$ is used to represent the set of all subsets.

III. EXPERIMENT AND RESULTS

This section is organized as follows. After the most impacted frequency band $\mathbb{B}_s$ for indoor positioning is found by SHAP, PCA, and statistical variance; the RSS-based PRF spectrum is collected in $\mathbb{B}_s$. GPR and other regressors are used to fit observation data and make predictions. This section highlights the experimental setup, phenomenal observation, and results.

A. Experimental Setup

Data collection is done in a living room scenario, which is illustrated in Fig. 3. In order to avoid the influence of human activity on the PRF spectrum, the host computer operator is fixed at the position near the host computer. There are other objects that may affect the PRF data, such as a television, WiFi router, printers, etc. are also marked in Fig. 3. The WiFi router
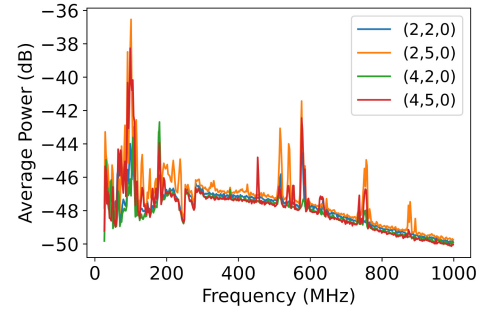

Fig. 4. Full frequency band PRF spectrum of $(2, 2, 0)$, $(2, 5, 0)$, $(4, 2, 0)$, and $(4, 5, 0)$.

or the host computer's Bluetooth module will not interfere directly with the PRF spectrum since they operate in bands other than $\mathbb{B}$. However, the electrical noise they generate and the material of their metal may still affect the PRF spectrum. An experimental scenario with a length of 6.15 m, a width of 4.30 m, and a height of 2.42 m is used as a preliminary verification of the PRF positioning. Ninety gridded positions as coordinates were set up in 3-D space for data collection.

According to the assumptions and derivations of frequency band selection and GPR presented in Section II, the system in this article can be generalized by Scikit-learn and SHAP toolkit under the TensorFlow framework. In PCA, the number of components is set to 10 to keep the ten components with the most significant variance. We prebuild a linear SVM classifier, which is used to classify samples at different positions. This classifier is only used for SHAP to explain the impact of different features on the linear SVM classifier model. The building of GPR and other regressors also benefits from the Scikit-learn toolkit for its usability, reliability, and simplicity.

B. Frequency Band Selection

According to Section II-B for the frequency band selection, we precollected the full frequency band data at four coordinates, e.g., $(2, 2, 0)$, $(2, 5, 0)$, $(4, 2, 0)$, and $(4, 5, 0)$ to find the frequency bands that have the most impact on positioning. Fig. 4 shows the full frequency band PRF spectrum for these four coordinates. It can be seen that there are minor differences in the PRF spectrum at different coordinates, which are difficult to visually distinguish. The difference in the PRF spectrum is not only due to different spatial coordinates but may also be due to other factors, such as sampling time, interference, electrical noise, etc. Therefore, it is necessary to use the frequency band selection algorithm to find the most impacted frequency band and then use a regressor to achieve positioning.

The ten most impacted frequencies found from SHAP, PCA, and statistical variance are summarized in Table III. It can be seen that all three methods give the similar most impacted frequencies, especially in the frequency 100. 8 MHz, all three methods give the same conclusion. SHAP also generates the visualization of the most impact frequencies, as shown in Fig. 5. It can be seen that the frequencies from 91.2 to 100.8 MHz have a higher Shapley value, that is, a higher impact on the model output. Also, in these particular frequencies, the impact on the model is higher when

TABLE III
TEN MOST IMPACT FREQUENCIES ARE FOUND FROM SHAP,
PCA, AND STATISTICAL VARIANCE

Ranking	$\mathbb{B}_{SHAP}$ (MHz)	$\mathbb{B}_{PCA}$ (MHz)	$\mathbb{B}_{Var}$ (MHz)	SHAP Impact (%)	PCA Impact (%)	Variance Impact (%)
1st	100.8	100.8	100.8	11.61	67.46	9.84
2nd	91.2	105.6	98.4	9.31	12.64	8.32
3rd	98.4	180.0	91.2	7.14	4.91	6.93
4th	105.6	103.2	103.2	3.55	1.94	3.72
5th	74.4	31.2	96.0	3.40	1.35	3.64
6th	88.8	636.0	576.0	3.39	1.13	3.05
7th	115.2	756.0	88.8	3.20	0.97	2.66
8th	110.4	31.2	105.6	2.08	0.74	2.53
9th	542.4	24.0	74.4	1.79	0.62	2.40
10th	84.0	756.0	84.0	1.54	0.51	2.22
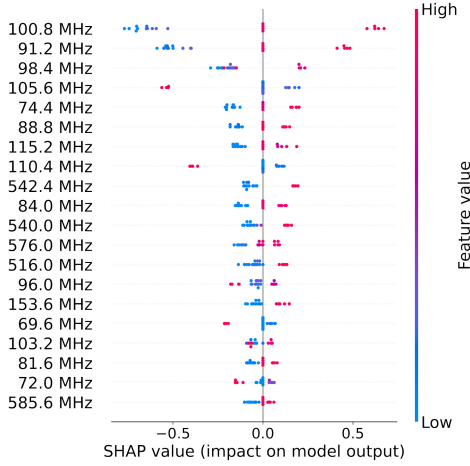
Fig. 5. Frequency ranking that impacts the positioning of linear SVM classifier is evaluated by SHAP.
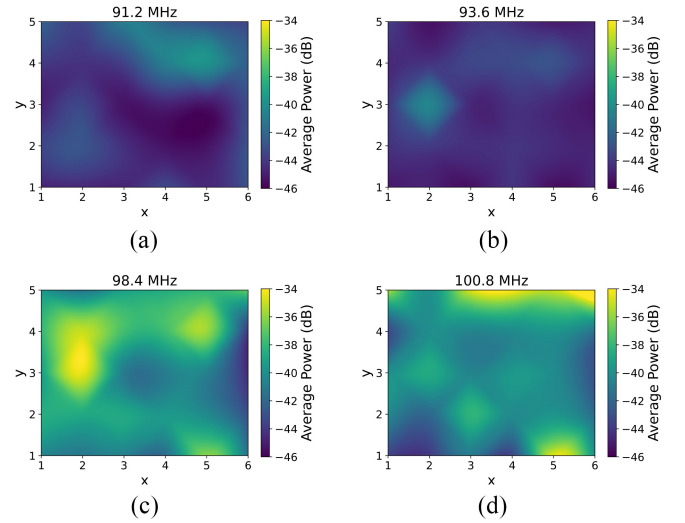

Fig. 6. Overall RSS distribution with the antenna is 0 m from the ground when the frequency is at (a) 91.2 MHz, (b) 93.6 MHz, (c) 98.4 MHz, and (d) 100.8 MHz. Figures are cubically interpolated to increase resolution.

the feature value is higher, which is shown by the color of the sample points. In addition to the SHAP visualization, Table III gives the percentage of the frequencies impact from SHAP, PCA, and statistical variance. For each frequency, SHAP impact is obtained by calculating the percentage of the Shapley value to the sum, PCA impact is obtained from the PCA explained variance, and variance impact is obtained from the percentage of the statistical variance to the sum. The selected frequency band $\mathbb{B}_s$ is obtained by Algorithm 1, where the similarity is equal to the sum of the three impacts of the corresponding frequencies. Therefore, we choose 91.2 to 100.8 MHz as the selected positioning center frequency band $\mathbb{B}_s$ with a step size of 2.4 MHz

$$\mathbb{B}_s(\text{MHz}) = \{91.2, 93.6, 96.0, 98.4, 100.8\}. \tag{18}$$

A total of five frequency corresponding average powers are used as the features of the data. The collection time for each frequency is 0.2 s. Hence, the sampling period for PRF positioning is only 1 s. The frequency band selection algorithm is one of the most critical feature extraction methods for PRF, which is able to reduce the number of features from 407 to 5. The advantages include fewer GPR model training resources, comparable accuracy, and especially the sampling speed increased by 98.77%.

C. RSS Distribution

For the GPR regressor, the time complexity of model fitting increases exponentially with the number of samples. Generally speaking, as the amount of data increases, the computing resources consumed will increase exponentially. GPR's ability to handle small data is surprising, so we limit the number of samples in the data set to less than 10 000. After the most impacted frequency band was determined, we collected 100 samples each at 90-gridded positions to research RSS distribution and PRF antenna positioning. Fig. 6 is used to show the distribution of the overall RSS in the scenario at different frequencies; while Fig. 7 highlights the similarities and differences of sample RSS collected from adjacent coordinates. Fig. 6 shows the overall RSS distribution at different frequencies with $z = 0$ as an example. It can be seen that at different frequencies, the average power RSS distribution is clustered at different positions in the indoor space, and the power levels are also different.

The usability and flexibility of GPR have been valued in recent studies, especially its ability to model in the real world. We solve the open question of whether GPR is suitable for the RSS-based PRF spectrum by observing the RSS distribution at different coordinates. Fig. 7 shows the RSS histogram of the sample PRF spectrum at different frequencies. It can be clearly seen that the RSS of different coordinates presents a Gaussian distribution, and various Gaussian distributions are distributed on the entire axis. We take (3, 3, 0.5) as a center point and use six points around it as test points to explore whether the adjacent coordinates will be confused. Taking Fig. 7(d) 100.8 MHz as an example, the RSS collected at the center point has a 99% overlap with the RSS collected at the test points (4, 3, 0.5), but they do not have any overlap at 91.2 MHz. Hence, GPR is able to estimate accurate coordinates as long as the RSS for both coordinates does not overlap at all five frequencies. Therefore, we propose GPS as a regressor for PRO-3DIPS to estimate coordinates for positioning.
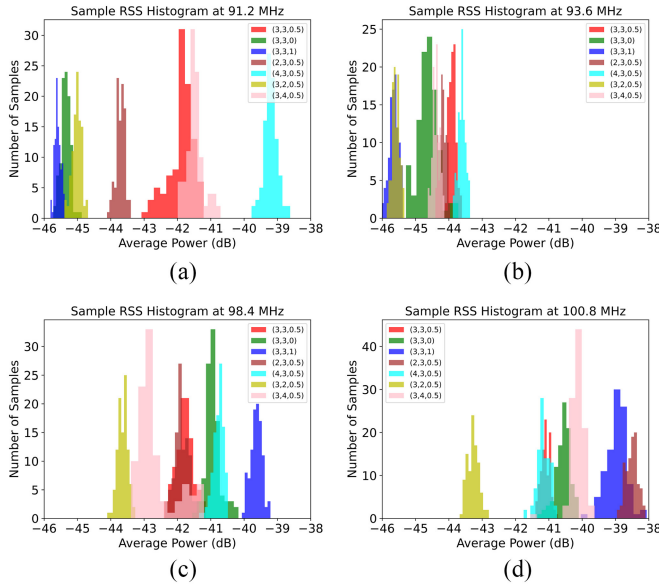
Fig. 7.   RSS histogram of PRF spectrum when the frequency is at (a) 91.2 MHz, (b) 93.6 MHz, (c) 98.4 MHz, and (d) 100.8 MHz.

TABLE IV
PERFORMANCE EVALUATION OF GPR AND SEVERAL REGRESSORS

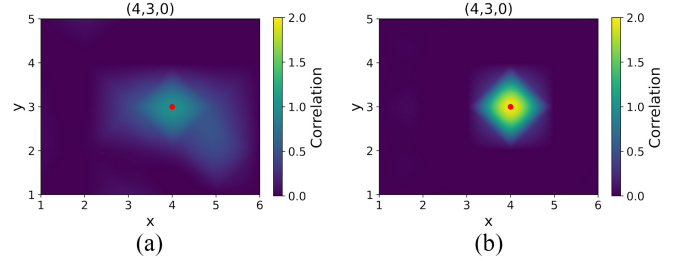| Regressor	RMSE (m)	R^2	95% CE (m)
$\mathrm{GPR}_{k_{\mathrm{RBF}}}$	0.367	0.978	0.779
$\mathrm{GPR}_{k_{\mathrm{Total}}}$	0.296	0.987	0.593
$\mathrm{GPR}_{k_{\mathrm{M}}}$	0.292	0.987	0.546
SVR	0.565	0.947	1.298
k-NN	0.311	0.985	0.532
DT	0.630	0.932	1.056
RFR	0.387	0.976	0.822
MLP	0.556	0.970	1.069
CNN	0.662	0.957	1.287
RNN	0.608	0.964	1.243

Fig. 8.   Spatial data correlation distribution is calculated by, (a) default k_M, (b) trained k_M. The target coordinates are $(4, 3, 0)$ represented by red dots.

D. PRF Positioning

After detailed observation and analysis of the RSS distribution, positioning experiments are conducted on the data set collected on 90-gridded positions. Since none of the models used in this article have been tuned, the data set is divided into training set and test set with a ratio of 0.7 and 0.3. In GPR, the upper and lower bounds of the length scale are limited to 0.01 and 100 to prevent overfitting and underfitting. In DL models, overfitting is prevented by adding a dropout layer of 0.2. Models are implemented on TensorFlow and scikit-learn, then trained on an Intel Core i9-10850K CPU @ 3.60 GHz, and a Nvidia GeForce RTX(TM) 3080 GPU.

The GPR model has a variety of optional kernels, as discussed in Section II-C. According to the similarity of observation $\boldsymbol{D}$ and predictive data $\boldsymbol{D}'$, it is a challenge to choose a suitable kernel. The kernel selection is largely dependent on the data differences of different coordinates. Two coordinates that are far apart should have less similarity. Ideally, the predictive data is only similar to the data corresponding to the same coordinate, which means that the kernel function should have a steep decay. Using prior knowledge, some kernels are not appropriate for the indoor positioning task, such as kernel k_{ESS} with periodic characteristics, which is also consistent with the experimental results. Table IV only shows three representative kernels with high performance as examples, e.g., a default kernel k_{RBF}, a total kernel k_{Total} including all kernels, and a highest performance kernel k_M.

It is expected that k_M has the highest performance because it has an anisotropic length scale and is steeper than k_{RBF}. It is worth noting that although k_{Total} also includes k_M itself, it is not prominent by comparison. This may be because the addition of other kernels makes other coordinates have greater weights for the predicted coordinates, which increases the variance of the weight distribution. Fig. 8 shows the correlation distribution of k_M with default parameters and k_M after

training. The hyperparameter of trained k_M is given by

$$k_M(\sigma = 1.41, \boldsymbol{l} = (0.11, 0.0946, 0.147, 0.132, 0.0951))$$
$$k_N(\text{noise level} = 0.00693). \tag{19}$$

It can be seen that the correlation distribution of the trained k_M kernel is strongly correlated with the predictive coordinate. However, the correlation of the default k_M kernel is widely distributed over adjacent coordinates.

To illustrate the excellent performance of GPR on the positioning regression problem, several regressors in the related literature are selected for comparison, and they are also integrated with the Scikit-learn toolkit. Since the 3-D positioning task is a multioutput problem, it is not suitable for some common regressors such as SVR. Although the Scikit-learn toolkit gives an extension as a multioutput regressor, it actually splits the multioutput regressor into multiple single-output regressors, which obviously reduces accuracy. SVR also uses the Matern kernel in our experiment. Other multioutput regressors were also chosen for comparison, including k-NN, decision tree (DT), random forest (RFR), multilayer perceptron (MLP), convolutional neural network (CNN), and recurrent neural network (RNN). It is worth noting that k-NN, DT, and RFR are all highly integrated and widely used models, and the parameters of their default models are suitable for most of the data. However, MLP, CNN, and RNN have multiple adjustable parameters and internal structures, which will significantly affect the accuracy. To preliminarily examine the ability of DL in PRF positioning regression, we set up three hidden layers, each with 128 units, the loss function of MSE, the optimizer of Adam, the learning rate of 0.01, and 200 epochs to observe their performance. All three types of DL use roughly similar structures and trainable parameters.

Table IV shows that several GPR models have candidate kernels and several other popular regressors. After GPR fitting
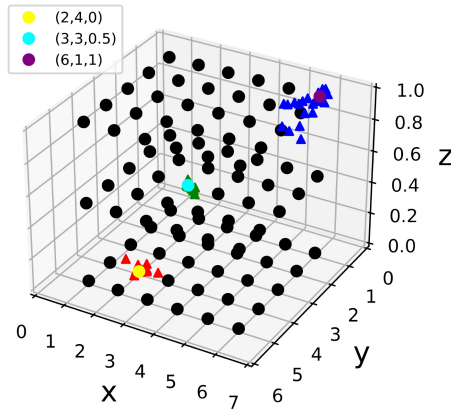
Fig. 9. GPR model prediction results for three test coordinates. The black dots represent the actual coordinates. The yellow, cyan, and purple dots are three randomly selected example coordinates, respectively, and the corresponding prediction results are represented by red, green, and blue triangles.
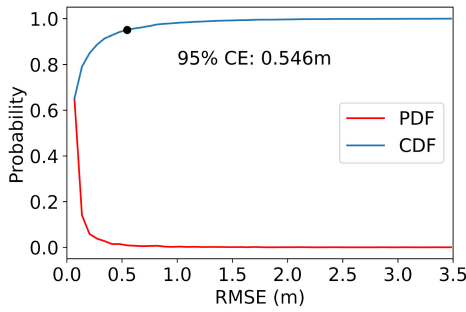

Fig. 10. RMSE versus probability curve predicted by GPR model.

and prediction on the test data set, we get an average RMSE of 0.292 m on the test data set and a coefficient of determination R^2 equal to 0.987. Fig. 9 gives the predicted results for three example coordinates. It can be seen that the prediction results are better, especially when the coordinates are in the center of the experiment scenario. The test coordinate $(6, 1, 1)$ farther from the center of the experiment scenario and closer to the wall has a larger error in its prediction.

Fig. 10 gives the curve of RMSE versus probability, i.e., PDF and CDF. It can be observed that the RMSE is equal to 0.546 m for 95% confidence, which means that for any prediction, we have 95% confidence that the prediction has an error of less than 0.546 m.

E. Test on Nontrained Positions

Generally speaking, the uncertainty of GPR model prediction is lower where the training data points are denser; and the model prediction uncertainty is higher in the area where the training data points are sparse. It is challenging to the uncertainty of the GPR model, which will be strongly reflected in the nontraining positions. To better demonstrate the performance of the proposed PRO-3DIPS, we conduct tests on nontrained positions. We randomly select one position from the 90-gridded positions as test coordinates, and the remaining positions are used as a training data set ten times. Fig. 11 shows the prediction results of these eight models at nontrained positions, where GPR has a lower average RMSE. It
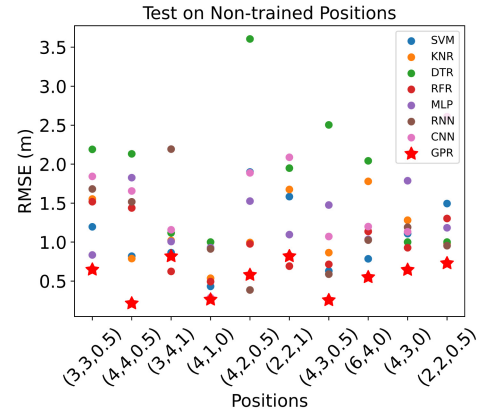

Fig. 11. Test on ten nontrained positions.

can be seen that the error of GPR is not very stable, which has almost twice the error range at different positions. Predictive instability may be due to the fact that the RSS in the scenario is not evenly distributed. It will produce significant changes in some areas due to small-scale fading, which is also one of the characteristics of PRF-based positioning systems.

IV. DISCUSSION

Our research provides initial evidence for PRF technology as a solution for obtaining indoor RSS distribution and 3-D positioning. It has been shown to have visualization and real-time application prospects. In this article, two major contributions have been highlighted: observation of RSS distribution and PRF technology for positioning. In this work, the RSS distribution is only used to achieve indoor positioning. However, it is expected that studying the RSS distribution can significantly assist and facilitate RF sensing techniques. For example, monitoring RSS distribution to detect building structures, demonstrate the pattern and distribution of interference in active RF sensing, develop other PRF sensing applications, remote sensing of the earth, etc. The definition of a PRF system in this article differs from that in the related literature. We highlight the definition of the PRF system that does not deploy new transmitters rather than other passive RFID papers that focus on the presence of an internal power source for the tag. The proposed PRO-3DIPS is able to use ambient SoOP for positioning without knowing any a priori information about possible existing transmitters. It is worth noting that the RF of broadcasting in the Detroit metropolitan area where the experimental scenario is located ranges from 88.1 to 107.9 FM [52], [53], which coincides with our $\mathbb{B}_s$. Therefore, we believe that around the Detroit metropolitan area, the frequency band most impacted by positioning will be fixed. Thus, the proposed PRO-3DIPS can be easily extended to other scenarios, such as classrooms, laboratories, factories, warehouses, etc. To the best of our knowledge, the novel work proposed in this article is the first work to realize 3-D indoor positioning via PRF technology.

Simple numerical comparisons with the techniques and performances mentioned in Table II are inaccurate since the RMSE is not only related to the proposed method but also
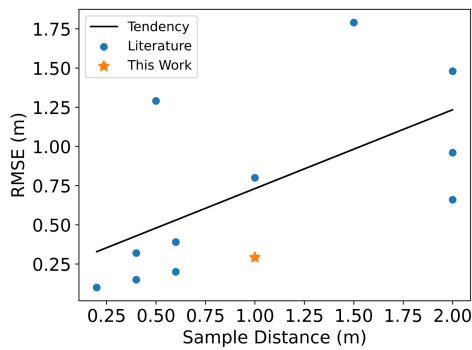
Fig. 12. Performance comparison with related literature.

to the experimental setup. For active RF technology, especially WiFi, the RMSE and performance of the system are also related to the number of transmitters. Our proposed PRO-3DIPS does not deploy any transmitters, which is one of it's advantages. To better illustrate the excellent performance of the PRO-3DIPS, considering that the RMSE is usually related to the sampling distance, the results of the proposed method compared with the literature are shown in Fig. 12. It can be seen that the proposed work is below the reference trend line, which means that the performance of the PRO-3DIPS is higher than most of the relevant literature. The PRO-3DIPS is only compared with other 2-D IPSs, for reasons other than obtaining better accuracy on more challenging tasks and, more importantly, because there are only a few 3-D positioning technologies currently available. These techniques have only the disadvantages of low accuracy, complex configuration, and difficulty to expand and are not recognized as generalized solutions.

V. CONCLUSION

This work presents an RSS-based PRF monitoring and 3-D IPS. After sampling the selected frequency band, comparable results are obtained according to the GPR model. After using the frequency band selection algorithm to find the most impacted frequency band, a GPR model is built by characterizing the RSS distribution in 3-D space to achieve positioning. We conducted a series of experiments on three evaluation criteria, and the results include RMSE of 0.292 m, coefficient of determination of 0.987, and 95% CE of 0.546 m. The proposed PRO-3DIPS is significantly better than the state-of-the-art, which can promote the wider use of SoOP.

Future work includes further verifying the PRO-3DIPS, including real-time, anti-interference capability, and large-area applications. For a positioning system, its real-time performance is one of the essential evaluation criteria. The real-time performance is initially discussed and improved in this article, that is, the improvement of the sampling rate from the frequency selection algorithm. Another optional parameter is to reduce the number of IQ samples mentioned in Eq. (1). In addition, the RTL-SDR device is selected as the PRF sensor in this article for low-cost consideration, and a higher performance SDR device can be used to develop a promising real-time positioning system. The anti-interference capability

of PRF is also a challenge. Previous work has confirmed that the PRF spectrum can be affected by human position and activity, and is also sensitive to metallic objects. Multisensor fusion may be a practical solution. This article proposes to use PRF for positioning and conducts preliminary experiments in the living room scenario. Further experiments are planned to extend the PRF positioning technology to larger area experimental scenarios, such as a university building.

REFERENCES

[1] F. Liu et al., "Survey on WiFi-based indoor positioning techniques," *IET Commun.*, vol. 14, no. 9, pp. 1372–1383, May 2020.
[2] B. Ezhumalai, M. Song, and K. Park, "An efficient indoor positioning method based on Wi-Fi RSS fingerprint and classification algorithm," *Sensors*, vol. 21, no. 10, p. 3418, Jan. 2021.
[3] J. C. Torres et al., "A low-cost visible light positioning system for indoor positioning," *Sensors*, vol. 20, no. 18, p. 5145, Jan. 2020.
[4] K. Gligorić, M. Ajmani, D. Vukobratović, and S. Sinanović, "Visible light communications-based indoor positioning via compressed sensing," *IEEE Commun. Lett.*, vol. 22, no. 7, pp. 1410–1413, Jul. 2018.
[5] A. Alarifi et al., "Ultra wideband indoor positioning technologies: Analysis and recent advances," *Sensors*, vol. 16, no. 5, p. 707, May 2016.
[6] X. Shan and Z. Shen, "Miniaturized UHF/UWB tag antenna for indoor positioning systems," *IEEE Antennas Wireless Propag. Lett.*, vol. 18, pp. 2453–2457, 2019.
[7] A. A. N. Shirehjini and S. Shirmohammadi, "Improving accuracy and robustness in HF-RFID-Based indoor positioning with Kalman filtering and Tukey smoothing," *IEEE Trans. Instrum. Meas.*, vol. 69, pp. 9190–9202, 2020.
[8] H. Xu, M. Wu, P. Li, F. Zhu, and R. Wang, "An RFID indoor positioning algorithm based on support vector regression," *Sensors*, vol. 18, no. 5, p. 1504, May 2018.
[9] S. Zhao, X.-P. Zhang, X. Cui, and M. Lu, "Optimal localization with sequential pseudorange measurements for moving users in a time-division broadcast positioning system," *IEEE Internet Things J.*, vol. 8, no. 11, pp. 8883–8896, Jun. 2021.
[10] S.-C. Yeh, W.-H. Hsu, W.-Y. Lin, and Y.-F. Wu, "Study on an indoor positioning system using Earth's magnetic field," *IEEE Trans. Instrum. Meas.*, vol. 69, pp. 865–872, 2020.
[11] A. Pandey, P. Tiwary, S. Kumar, and S. K. Das, "Adaptive mini-batch gradient-ascent-based localization for indoor IoT networks under Rayleigh fading conditions," *IEEE Internet Things J.*, vol. 8, no. 13, pp. 10665–10677, Jul. 2021.
[12] R. Adhikary and J. N. Daigle, "RSS based localization in Rayleigh fading environment," in *Proc. IEEE Wireless Commun. Netw. Conf.*, 2016, pp. 1–6.
[13] T. Jiang, D. Chen, C. Ni, and D. Qu, *OQAM/FBMC for Future Wireless Communications: Principles, Technologies and Applications*. Cambridge, MA, USA: Elsevier, 2017.
[14] D. R. Jensen, "Gaussian approximation to bivariate Rayleigh distributions," *J. Stat. Comput. Simul.*, vol. 4, no. 4, pp. 259–267, Jan. 1976.
[15] V. Moghtadaiee, A. G. Dempster, and S. Lim, "Indoor localization using FM radio signals: A fingerprinting approach," in *Proc. Int. Conf. Indoor Position. Indoor Navig.*, 2011, pp. 1–7.
[16] L. Yuan, H. Chen, R. Ewing, and J. Li, "Passive radio frequency-based 3D indoor positioning system via ensemble learning," in *Dynamic Data Driven Applications Systems* (Lecture Notes in Computer Science). Heidelberg, Germany: Springer, 2022.
[17] Z. Tan, H. Qin, L. Cong, and C. Zhao, "Positioning using IRIDIUM satellite signals of opportunity in weak signal environment," *Electronics*, vol. 9, no. 1, p. 37, 2019.
[18] A. Nessa, B. Adhikari, F. Hussain, and X. N. Fernando, "A survey of machine learning for indoor positioning," *IEEE Access*, vol. 8, pp. 214945–214965, 2020.
[19] S. R. Jondhale, V. Mohan, B. B. Sharma, J. Lloret, and S. V. Athawale, "Support vector regression for mobile target localization in indoor environments," *Sensors*, vol. 22, no. 1, p. 358, Jan. 2022.
[20] A. Datta, M. J. Augustin, N. Gupta, S. R. Viswamurthy, K. M. Gaddikeri, and R. Sundaram, "Impact localization and severity estimation on composite structure using fiber Bragg grating sensors by least square support vector regression," *IEEE Sensors J.*, vol. 19, no. 12, pp. 4463–4470, Jun. 2019.

[21] H. Cao et al., "WiFi RTT indoor positioning method based on Gaussian process regression for harsh environments," *IEEE Access*, vol. 8, pp. 215777–215786, 2020.

[22] Y.-J. Park, P. M. Tagade, and H.-L. Choi, "Deep Gaussian process-based Bayesian inference for contaminant source localization," *IEEE Access*, vol. 6, pp. 49432–49449, 2018.

[23] H. Xu, Y. Ding, P. Li, R. Wang, and Y. Li, "An RFID indoor positioning algorithm based on Bayesian probability and K-nearest neighbor," *Sensors*, vol. 17, no. 8, p. 1806, Aug. 2017.

[24] S. Sadowski, P. Spachos, and K. N. Plataniotis, "Memoryless techniques and wireless technologies for indoor localization with the Internet of Things," *IEEE Internet Things J.*, vol. 7, no. 11, pp. 10996–11005, Nov. 2020.

[25] P. Mahida, S. Shahrestani, and H. Cheung, "Deep learning-based positioning of visually impaired people in indoor environments," *Sensors*, vol. 20, no. 21, p. 6238, Jan. 2020.

[26] Z. Munadhil, S. K. Gharghan, A. H. Mutlag, A. Al-Naji, and J. Chahl, "Neural network-based alzheimer's patient localization for wireless sensor network in an indoor environment," *IEEE Access*, vol. 8, pp. 150527–150538, 2020.

[27] C.-Y. Yao and W.-C. Hsia, "An indoor positioning system based on the dual-channel passive RFID technology," *IEEE Sensors J.*, vol. 18, no. 11, pp. 4654–4663, Jun. 2018.

[28] W. Sun, M. Xue, H. Yu, H. Tang, and A. Lin, "Augmentation of fingerprints for indoor WiFi localization based on Gaussian process regression," *IEEE Trans. Veh. Technol.*, vol. 67, no. 11, pp. 10896–10905, Nov. 2018.

[29] G. Zhang, P. Wang, H. Chen, and L. Zhang, "Wireless indoor localization using convolutional neural network and Gaussian process regression," *Sensors*, vol. 19, no. 11, p. 2508, Jan. 2019.

[30] F. Li, M. Liu, Y. Zhang, and W. Shen, "A two-level WiFi fingerprint-based indoor localization method for dangerous area monitoring," *Sensors*, vol. 19, no. 19, p. 4243, Jan. 2019.

[31] M. T. Hoang et al., "A soft range limited K-nearest neighbors algorithm for indoor localization enhancement," *IEEE Sensors J.*, vol. 18, no. 24, pp. 10208–10216, Dec. 2018.

[32] J. Hu, D. Liu, Z. Yan, and H. Liu, "Experimental analysis on weight K-nearest neighbor indoor fingerprint positioning," *IEEE Internet Things J.*, vol. 6, no. 1, pp. 891–897, Feb. 2019.

[33] L. Zhang et al., "WiFi-based indoor robot positioning using deep fuzzy forests," *IEEE Internet Things J.*, vol. 7, no. 11, pp. 10773–10781, Nov. 2020.

[34] B.-H. Lee, K.-M. Park, Y.-H. Kim, and S.-C. Kim, "Hybrid Approach for indoor localization using received signal strength of dual-band Wi-Fi," *Sensors*, vol. 21, no. 16, p. 5583, Jan. 2021.

[35] Y. Zhuang, J. Yang, Y. Li, L. Qi, and N. El-Sheimy, "Smartphone-based indoor localization with Bluetooth low energy beacons," *Sensors*, vol. 16, no. 5, p. 596, May 2016.

[36] Z. Chen and J. Wang, "GROF: Indoor localization using a multiple-bandwidth general regression neural network and outlier filter," *Sensors*, vol. 18, no. 11, p. 3723, Nov. 2018.

[37] Q. Zou, Q. Sun, L. Chen, B. Nie, and Q. Li, "A comparative analysis of LiDAR SLAM-based indoor navigation for autonomous vehicles," *IEEE Trans. Intell. Transp. Syst.*, vol. 23, no. 7, pp. 6907–6921, Jul. 2022.

[38] M. Shu, G. Chen, and Z. Zhang, "3D point cloud-based indoor mobile robot in 6-DoF pose localization using a Wi-Fi-aided localization system," *IEEE Access*, vol. 9, pp. 38636–38648, 2021.

[39] Y.-S. Chen, C.-S. Hsu, and R.-S. Chung, "A semi-supervised 3D indoor localization using multi-kernel learning for WiFi networks," *Sensors*, vol. 22, no. 3, p. 776, Jan. 2022.

[40] L. Zhang and H. Wang, "3D-WiFi: 3D localization with commodity WiFi," *IEEE Sensors J.*, vol. 19, no. 13, pp. 5141–5152, Jul. 2019.

[41] X. Liu et al., "Accurate localization of tagged objects using mobile RFID-augmented robots," *IEEE Trans. Mobile Comput.*, vol. 20, no. 4, pp. 1273–1284, Apr. 2021.

[42] J. Liu et al., "Human occupancy detection via passive cognitive radio," *Sensors*, vol. 20, no. 15, p. 4248, Jan. 2020.

[43] H. Mu, R. Ewing, E. Blasch, and J. Li, "Human subject identification via passive spectrum monitoring," in *Proc. IEEE Nat. Aerosp. Electron. Conf. (NAECON)*, 2021, pp. 317–322.

[44] S. Yang, L. Yuan, and J. Li, "Extraction and denoising of human signature on radio frequency spectrum," in *Proc. IEEE Int. Conf. Consum. Electron. (ICCE)*, 2023, pp. 1–6.

[45] L. Yuan et al., "Interpretable passive multi-modal sensor fusion for human identification and activity recognition," *Sensors*, vol. 22, no. 15, p. 5787, Aug. 2022.

[46] H. Mu, J. Liu, R. Ewing, and J. Li, "Human indoor positioning via passive spectrum monitoring," in *Proc. 55th Annu. Conf. Inf. Sci. Syst. (CISS)*, 2021, pp. 1–6.

[47] W. Nie, Z.-C. Han, M. Zhou, L.-B. Xie, and Q. Jiang, "UAV detection and identification based on WiFi signal and RF fingerprint," *IEEE Sensors J.*, vol. 21, no. 12, pp. 13540–13550, Jun. 2021.

[48] I. T. Jolliffe and J. Cadima, "Principal component analysis: A review and recent developments," *Philos. Trans. Roy. Soc. A, Math. Eng. Sci.*, vol. 374, no. 2065, Apr. 2016, Art. no. 20150202.

[49] S. M. Lundberg and S.-I. Lee, "A unified approach to interpreting model predictions," in *Proc. Int. Conf. Adv. Neural Inf. Process. Syst.*, vol. 30, 2017, pp. 4768–4777.

[50] C. E. Rasmussen and C. K. Willia, *Gaussian Processes in Machine Learning*. Cambridge, MA, USA: MIT Press, 2006.

[51] D. Duvenaud. "The kernel cookbook: Advice on covariance functions." cs.toronto.edu. Accessed: May 15, 2022. [Online]. Available: https://www.cs.toronto.edu/~duvenaud/cookbook/

[52] "List of radio stations in Michigan." wikipedia.org. Accessed: Jun. 9, 2022. [Online]. Available: https://en.wikipedia.org/wiki/List_of_radio_stations_in_Michigan

[53] "There are 80 radio stations that may be within distant listening range of 48309 (Rochester Hills, MI). (42° 40' 01" N, 83° 10' 55" W)." radio-locator.com. Accessed: Jun. 9, 2022. [Online]. Available: https://radio-locator.com/cgi-bin/locate?select=city&city=48309&x=0&y=0

Liangqi Yuan (Student Member, IEEE) received the B.E. degree from Beijing Information Science and Technology University, Beijing, China, in 2020, and the M.S. degree from Oakland University, Rochester, MI, USA, in 2022. He is currently pursuing the Ph.D. degree with the School of Electrical and Computer Engineering, Purdue University, West Lafayette, IN, USA.

His research interests are in the areas of sensors, the Internet of Things, signal processing, and machine learning.

Houlin Chen is currently pursuing the B.S. degree (Hons.) with the Faculty of Arts and Science, University of Toronto, Toronto, ON, Canada.

Throughout her university research, she engaged in multiple projects encompassing various aspects, such as Bayesian estimation for distributional differences, multiple linear regression for multivariate data analysis, and Monte Carlo approximations. She is currently undertaking an internship in marketing data analysis with AP Lazer Canada Mfg. Inc., Windsor, ON, Canada. Her research interests include Bayesian statistics, data analysis, and machine learning.

Robert Ewing (Fellow, IEEE) received the bachelor's degree in electrical engineering and the master's degree in physics from the University of Cincinnati, Cincinnati, OH, USA, and the Ph.D. degree in electrical engineering from the University of Dayton, Dayton, OH, USA.

He began his career with the Propulsion Laboratory, Wright-Patterson Air Force Base, Dayton, with the development of high-speed jet engine control systems. He later held the position of a Medical Research Scientist with the Aerospace Medical Research Laboratory, Dayton, and an Instructor with the Air Force Institute of Technology, Dayton, where he co-pioneered the use of quantitative feedback theory for the design of robust analog and digital flight control and aircraft ejection systems. During the early 1990s, he led the Wright Laboratory's Solid State Electronic Devices Directorate's research in the area of mixed-signal hardware description language (VHDL-AMS) for microelectronic VLSI digital design, the IEEE VHDL standards, and formal verification of digital designs. He became the Director of the Computer Engineering Research Consortium, a research center composed of universities, industry, and graduate students for the innovative development of mixed-signal design methodology and tools, real-time wavelet transforms for video and radar applications, and spiking neural networks for pattern recognition. He has authored over 140 journal and conference publications.

Dr. Ewing chaired numerous international IEEE conferences, an Adjunct Professor and an Associate Editor of *Electronic Letters* and *Institute of Engineering and Technology*, and the Board of Governors and the Executive Director of the IEEE Aerospace and Electronics Systems Society.

Erik P. Blasch (Fellow, IEEE) received the B.S. degree in mechanical engineering from the Massachusetts Institute of Technology, Cambridge, MA, USA, and the Ph.D. degree in electrical engineering from Wright State University, Dayton, OH, USA, in addition to numerous master's degrees in mechanical engineering, industrial engineering, electrical engineering, medicine, military studies, and economics.

He is a Program Officer with the Air Force Research Laboratory, Arlington, VA, USA. Additionally, his assignments include Colonel (ret) in the USAF reserves, Rome, NY, USA, an Adjunct Associate Professor and a President of professional societies. His areas of research include information-fusion performance evaluation, image fusion, avionics, and human–machine integration; compiling over 125 journal papers, 500 peer-reviewed publications, 45 patents, and eight books.

Dr. Blasch is a Fellow of AIAA (aerospace), MSS (sensing), and SPIE (optical) societies.

Jia Li (Senior Member, IEEE) received the B.S. degree in electronics and information systems from Peking University, Beijing, China, in 1996, and the M.S.E. and Ph.D. degrees in electrical engineering from the University of Michigan at Ann Arbor, Ann Arbor, MI, USA, in 1997 and 2002, respectively.

She has been a Faculty Member with the School of Engineering and Computer Science, Oakland University, Rochester, MI, USA, since 2002. She has authored/coauthored over 60 referred publications, including one book. Her past and current researches are sponsored by NSF, NIH, General Motors, Fiat Chrysler, Ford, National Research Council, and Air Force Office of Scientific Research. Her research interests are in the areas of statistical learning and signal processing with applications in radar, sensor fusion, communications, and biomedical imaging.

Dr. Li serves as a member of technical committees of several international conferences and workshops, and a regular reviewer of a number of international journals.